A physics-based interpretation of the slip-wall LES model

By X. I. A. Yang, S. Bose AND P. Moin

1. Motivation and objectives

The need for LES wall models comes from the strict near-wall-resolution requirements of a wall-resolved LES (Chapman 1979; Choi & Moin 2012), the limited computational power and the need for high-fidelity numerical solutions in real-world engineering practices. Conducting large-eddy simulations (LES) implies the use of LES filters, whose sizes are commensurate with the local LES grid spacing. For wall-modeled LES (WMLES), where the grid spacing in the wall-normal direction scales with the boundary layer height, the near-wall turbulence is not resolved and is filtered. Because of this filtering, the no-slip condition does not apply at the wall; and the wall boundary conditions are supplied by LES wall models.

In general, wall models for a WMLES can be of Dirichlet, Neumann or Robin type (see Piomelli & Balaras (2002) for a review of commonly used LES wall models). A Dirichlet-type wall model provides a slip velocity u_w at the (virtual) wall (Bazilevs & Hughes 2007; Chung & Pullin 2009). With the slip velocity and a non-vanishing eddy viscosity at the (virtual) wall, the calculation of the shear stress at the wall is no different from that in the bulk region. Neumann-type models directly provide the wall shear stress. The velocity at the wall is not explicitly modeled. This type of model is probably the most intuitive and most commonly used in WMLES. Neumann-type models include the algebraic equilibrium wall models (Schumann 1975; Porté-Agel *et al.* 2000), the algebraic integral wall model (Yang *et al.* 2015), the equilibrium and non-equilibrium zonal wall models (Balaras & Benocci 1994; Park & Moin 2014) and a number of models that rely on optimal control and data mining (Nicoud *et al.* 2001; Templeton *et al.* 2006). Recently, Bose & Moin (2014) proposed to use a Robin-type wall closure

$$u_i - l_p \partial u_i / \partial y = 0, \tag{1.1}$$

where u_i is a non-zero slip velocity at the wall, the subscript $i = 1, 2, 3$ denotes the streamwise, wall-normal and spanwise directions, respectively and l_p is a length scale. As was rigorously proved in Bose & Moin (2014), the slip-wall formalism conforms with the use of the differential filter in LES (see Bose & Moin (2014) for a discussion on the differential filter). It is not clear, however, how the physics is captured by the slip-wall model.

In this work, we provide a physics-based interpretation of this slip-wall closure. We show first that the Robin-type wall closure in Eq. (1.1) is compatible with any LES filter, and second that the slip-wall model formalism can also be motivated physically with RANS-type equilibrium arguments. The possibility of explicitly accounting for the non-equilibrium effects is briefly discussed. The model performance is then compared with that of the algebraic wall model and the integral wall model in the context of turbulent channel flows. In addition to the mean flow and the variance, we compare the probability density function (PDF) of the wall shear stress in the WMLES with that

from a filtered direct numerical simulation (DNS). Throughout the article we use x, y, z for the streamwise, wall-normal, and spanwise directions and u, v, w for the streamwise, wall-normal and spanwise velocities.

2. A physics-based interpretation of the slip-wall model

The Robin-type LES wall closure takes the following form

$$\left[u - l_p \frac{\partial u}{\partial y}\right]_{y=0} = 0. \tag{2.1}$$

In this section, we provide a physics-based interpretation of this LES wall closure. We begin with the log law

$$\frac{\langle u \rangle}{u_\tau} = \frac{1}{\kappa} \ln\left(\frac{y}{y_o}\right), \tag{2.2}$$

where κ is the Karman constant, y_o is the viscous/roughness length scale, u_τ is the friction velocity and $\langle\cdot\rangle$ denotes ensemble averaging. The algebraic equilibrium wall model imposes this log scaling locally and instantaneously. Imposing the log scaling at the first (or second, third, etc, depending on the implementation (Kawai & Larsson 2012)) grid point away from the wall leads to

$$u_\tau = \frac{\kappa u_{\mathrm{LES}}}{\ln(\Delta_y/y_o)}, \tag{2.3}$$

where u_{LES} is the LES velocity, Δ_y is distance of the LES grid point from the wall. Imposing the log law instantaneously, the non-equilibrium effects are neglected as a consequence, resulting

$$\widetilde{uv} - \tilde{u}\tilde{v} = \nu_T \frac{\partial u_{\mathrm{LES}}}{\partial y} = u_\tau^2, \tag{2.4}$$

where ν_T is the eddy viscosity. Substituting Eq. (2.3) with Eq. (2.4), we have

$$u_{\mathrm{LES}} - \left[\frac{\ln(\Delta_y/y_o)\nu_T}{\kappa u_\tau}\right] \frac{\partial u_{\mathrm{LES}}}{\partial y} = 0. \tag{2.5}$$

Equation (2.5) conforms with the form of a Robin boundary condition and we have

$$l_p = \frac{\ln(\Delta_y/y_o)\nu_T}{\kappa u_\tau}. \tag{2.6}$$

For a typical WMLES, in which the first LES grid point is in the log region, invoking the mixing length model for the eddy viscosity,

$$\nu_T = \kappa \Delta_y u_\tau, \tag{2.7}$$

Eq. (2.6) leads to

$$l_p = \Delta_y \log(\Delta_y/y_o). \tag{2.8}$$

Equations (2.5)-(2.6) physically justify the use of a Robin-type condition in a typical WMLES.

3. The slip-wall model

3.1. *Equilibrium slip-wall model*

The interpretation in Section 2 can be tested in a WMLES context. To do that we impose

$$u - l_p \frac{\partial u}{\partial y} = 0, \quad w - l_p \frac{\partial w}{\partial y} = 0, \quad v = 0 \tag{3.1}$$

at the wall with l_p from Eq. (2.8) and $\nu_T = \kappa u_\tau \Delta_y$. This Robin-type wall model imposes a non-penetration condition, therefore, the momentum loss at the wall is entirely due to $\nu_T \partial u/\partial y$. This is quite different from Bose & Moin (2014), in which a penetration condition is used and part of the momentum loss is due to a non-zero Reynolds stress at the wall. As discussed before, this work provides a physical basis for the Robin-type boundary condition in general, so we do not necessarily need to conform with the exact form used in Bose & Moin (2014).

3.2. *Accounting for non-equilibrium effects*

The discussion in Section 2 was based on equilibrium considerations. The non-equilibrium effects can be explicitly accounted for by including explicitly a non-equilibrium correction to the modeled wall shear stress according to

$$\tau_{w,x}^{NE} = \tau_{w,x}^{E} + \tau_{w,x}^{c}. \tag{3.2}$$

The subscript x denotes the stress in the x direction. The superscript E denotes equilibrium and NE denotes non-equilibrium. The wall stress in the spanwise direction can be corrected in the same manner. Following Yang *et al.* (2015), the non-equilibrium correction $\tau_{w,x}^{c}$ is

$$\tau_{w,x}^{c} = r \left[\int_{y=0}^{\Delta_y} -\frac{\partial p}{\partial x} - \frac{du}{dt} dy \right], \tag{3.3}$$

where $d\cdot/dt$ is the material derivative, p is the dynamic pressure, the pre-factor r matches the time scale of the resolved eddies (of scale Δ_y) and the time scale of the filtered wall shear stress. Following Yang *et al.* (2015), we take

$$r = \frac{T_c}{T_w}, \tag{3.4}$$

where $T_c = \Delta_y / u_{\mathrm{LES}}$ is the convective time scale, $T_w = \Delta_y/(\kappa u_\tau)$ is the time scale for the disturbance at $y = \Delta_y$ to reach $y = 0$. Because of the use of LES filters, the LES flow field is resolved by the grids. Hence, $u \approx u_w + (u_{\mathrm{LES}} - u_w)\, y/\Delta_y$, $p \approx p_w + (p_{\mathrm{LES}} - p_w)\, y/\Delta_y$ for $0 < y < \Delta_y$; besides, because Δ_y does not depend on t, x, y, z, the temporal and spatial derivatives can be taken out of the integral. The integration in Eq. (3.3) is trivial. This is rather different from Yang *et al.* (2015). In Yang *et al.* (2015), the LES filter did not act on the wall-normal direction and the subgrid flow field needed to be reconstructed. As a result, integrating the filtered momentum equation is quite non-trivial for Yang *et al.* (2015).

In this work, Eq. (3.3) is only used to supplement the slip-wall model (see Section 4), but it is potentially applicable to any equilibrium-type wall model, including the commonly used algebraic equilibrium wall model and the zonal equilibrium wall model. Testing such corrected models is beyond the scope of this work and is left to future investigations.

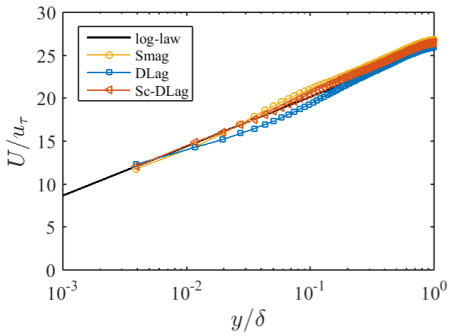

FIGURE 1. Mean velocity profile for WMLES. The sub-grid stress is modeled using the standard constant coefficient Smagorinsky model (Smag), the dynamic Lagrangian averaged model(DLag) and the scale-dependent version of the dynamic Lagrangian averaged model (Sc-DLag). The equilibrium wall model is used for near-wall closure. The grid size of the LES in this plot is 128^3. The detailed LES setup is discussed in detail in Section 4.1.

4. Wall-modeled LES

We present WMLES results in this section. The code used here is the open-source LES code LESGO (publically available on github). Details of this pseudo-spectral code can be found in Bou-Zeid *et al.* (2005) and Anderson & Meneveau (2011). The SGS model used in this study is the dynamic scale-dependent Lagrangian Smagorinsky model (Bou-Zeid *et al.* 2005). The WMLES results are found to be fairly insensitive to the sub-grid stress (SGS) model such as the dynamic Smagorinsky model (Germano *et al.* 1991), the dynamic Lagrangian Smagorinsky model (Meneveau *et al.* 1996) and the dynamic scale-dependent Lagrangian Smagorinsky model. These findings for the equilibrium wall model are presented in Figure 1 for the equilibrium wall model. Results for the algebraic integral wall model and the non-penetrating slip-wall model are similar and are not shown. For brevity, we present only the dynamic scale-dependent Lagrangian Smagorinsky model results. We compare the performance of four LES wall models, the algebraic equilibrium wall model (Moeng 1984), the integral wall model (Yang *et al.* 2015), the equilibrium slip-wall model (Eq. (3.1)) and the non-equilibrium slip-wall model (Eq. (3.2)). Both the algebraic equilibrium model and the integral wall model are readily available in the code. For equilibrium-type wall models, additional $x - z$ filtering is applied at $y = \Delta_y$ (see Moeng (1984) for a detailed discussion on the necessity of this additional filtering). We conduct this additional filtering for the algebraic wall models and the two Robin-type wall models.

4.1. *LES setup*

The flow configuration is a half-channel. We impose a constant pressure gradient. The friction velocity u_τ is known from $u_\tau = \sqrt{-1/\rho \partial \langle p \rangle / \partial x}$, where ρ is the fluid density. A symmetric boundary condition is used on the top boundary. Spanwise and streamwise periodicities are imposed. The computational domain is of size $2\pi \times 1 \times 2\pi$ in the x, y, z directions, respectively. The half-channel height is 1. To study the effects of grid resolution, we use two mesh sizes, 64^3 and 128^3. Uniform grid spacing is used in all directions. As will be clear from the following discussion, both the computational domain size and the grid size are reasonably large for the purpose of this work, although early LES studies by Stevens *et al.* (2014) suggested a domain size of $6\pi \times 1 \times 3\pi$ and a mesh size of $2048 \times 256 \times 1024$ for a faithful prediction of the variance.

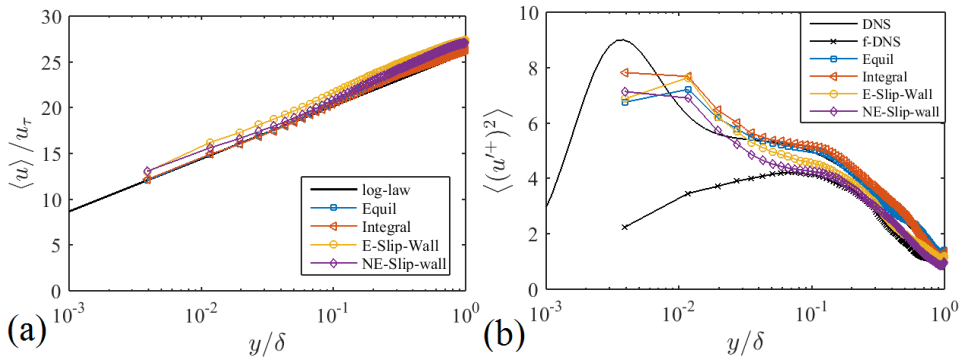

FIGURE 2. (a) Mean velocity profiles plotted against the wall-normal distance. δ is the half-channel height. The log-law corresponds to $U/u_\tau = 1/\kappa \log(yu_\tau/\nu) + B$, with $\kappa = 0.4$, $B = 5$. Equil is the algebraic equilibrium wall model, Integral is the integral wall model, E-Slip-Wall is the equilibrium slip-wall model, NE-Slip-Wall is the non-equilibrium slip-wall closure and f-DNS is the filtered DNS. (b) Same as (a) but for the streamwise variance.

The flow is at a Reynolds number $\mathrm{Re}_\tau = 4200$, where $\mathrm{Re}_\tau = \delta u_\tau/\nu$ is the friction Reynolds number. A full-channel DNS database at this Reynolds number is publicly available (Lozano-Durán & Jiménez 2014). The viscous length scale in the wall model is $y_o = \nu/u_\tau \exp(-\kappa B)$, where $B = 5$, $\kappa = 0.4$.

4.2. *Effects of wall models*

In Figure 2(a), we plot the LES velocity profiles against the wall-normal distance on a semi-log scale. For all the LES in Figure 2, we have used a grid of size 128^3. Both the equilibrium and non-equilibrium slip-wall models lead to slightly elevated mean velocity profiles. For various types of wall-bounded flows such as channel flows, pipe flows, boundary layers, etc., the mean profiles in the log region generally follow the log law closely; however, for the bulk region, the wake function (Coles 1956) depends quite a lot on the flow configuration (Marusic *et al.* (2013)). Hence, here we prefer to compare the LES results with the log law. As is seen from Figure 2, reasonable agreement with the log law is found for all wall models.

In Figure 2(b), we plot the variance of the streamwise velocity fluctuations against the wall-normal distance. At high Reynolds number, the variance follows a logarithmic scaling in the log region. At this Reynolds number ($\mathrm{Re}_\tau = 4200$), one can barely find a log region in the variance. The DNS results are therefore included for comparison. LES solves the filtered Navier-Stokes (NS) equation. For a fair comparison, $\langle u'^2 \rangle$ for the filtered DNS (coarse-grain DNS $\Delta x^+ \times \Delta y^+ \times \Delta z^+ \approx 200 \times 32.8 \times 200$) is included as well. In the near-wall region, $\langle u'^2 \rangle$ in WMLES is fairly comparable with the DNS data. The filtered DNS is less energetic. The DNS results and the filtered DNS results are quite similar in the bulk region. Differences between models can nevertheless be discerned. The results of Robin-type wall models align closely with the filtered DNS results. The integral wall model results, on the other hand, agree with the DNS data.

From Figure 2, we conclude first that the physics-based interpretation in Section 2 is reasonable and second that Robin-type models are generally an alternative to the Neumann-type models for LES wall closure.

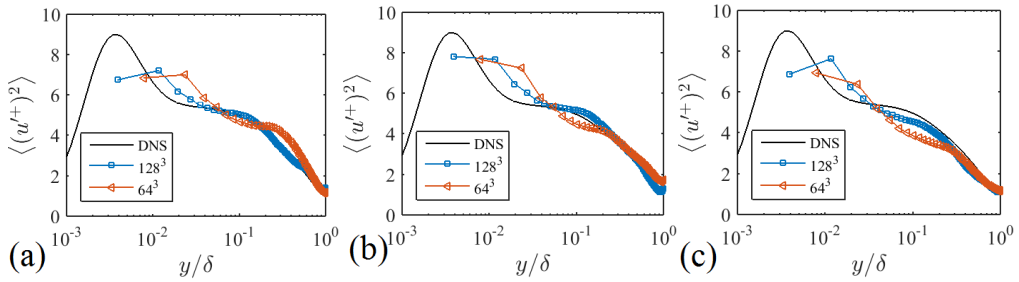

FIGURE 3. Variance of the streamwise velocity fluctuations plotted against the wall-normal distance for (a) the algebraic equilibrium wall model, (b) the integral wall model, (c) the equilibrium slip-wall model. DNS data are shown for comparison.

4.3. *Effects of grid resolution*

For the two grid resolutions investigated, i.e., grid sizes of 64^3, 128^3 for a domain size of $2\pi \times 1 \times 2\pi$, we find no difference in the mean velocity. Results of the mean flow are therefore not shown for brevity. In figure 3(a–c), we plot the variance of the streamwise fluctuations against the wall-normal distance for the algebraic equilibrium wall model, the integral wall model and the equilibrium slip-wall model, respectively. With sufficient grid resolution (in this case, with a grid size of 128^3), the results are fairly insensitive to the choice of the wall models, but with a coarse grid (in this case, 64^3), the wall model makes a difference. The expected grid convergence for the variance is from $y = \delta$ to the wall. That is to say, as we refine the mesh, we expect that the variance in the bulk region converges first to the DNS result and then the log region. This is because for $\left\langle u'^2 \right\rangle$ at y, only eddies with their characteristic length scales larger than $O(y)$ are statistically significant (see Townsend (1976); Woodcock & Marusic (2015); Yang *et al.* (2016*a*,*b*) for detailed discussion). This is seen for the integral wall model and the equilibrium slip-wall model, but not for the algebraic equilibrium wall model, suggesting that for a coarse-grid WMLES the integral wall model and the slip-wall model have an edge over the algebraic equilibrium wall model.

4.4. *Probability density function of the streamwise wall shear stress*

In Figure 4, we plot the instantaneous wall shear stress from the filtered DNS and the WMLES. Although the streaky pattern exists independent of the wall closure used, the spatial distribution of the fluctuating wall stress depends very much on the choice of wall models.

In Figure 5 we compare the wall stress PDF. The PDF from the LES using the integral wall model is in near agreement with the wall stress PDF in the filtered DNS. This is not entirely unexpected considering the success of the integral wall model in the *a priori* test in Graham *et al.* (2016). Compared to the filtered DNS, the wall stress PDF resulting from the equilibrium wall model is slightly less peaked and the wall stress PDF resulting from the equilibrium slip-wall model is slightly more peaked. This is because for equilibrium wall model $\tau_{w,x} \sim u_\tau^2 \sim u_{\mathrm{LES}}^2$ and for the slip-wall model $\tau_{w,x} \sim \nu_T \partial u/\partial y \sim \nu_T u_{\mathrm{LES}} \sim u_{\mathrm{LES}}$; the PDF of u_{LES}^2 is certainly less peaked than that of u_{LES}. Last, by including the non-equilibrium effects, the wall stress PDF moves toward that of the filtered DNS. The wall stress PDF from the DNS is included for comparison; although it is not expected with typical LES resolutions, this PDF can be reproduced.

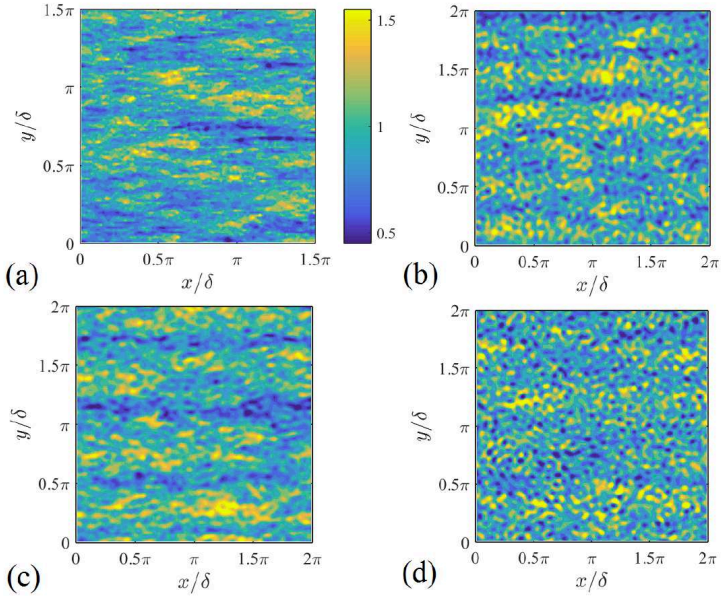

FIGURE 4. Contour plots of the normalized instantaneous streamwise wall shear stress, $\tau_{w,x}/u_\tau^2$ from (a) the filtered DNS (b) the LES modeled by the equilibrium wall model (c) the integral wall model and (d) the non-equilibrium slip-wall model. All LES cases are run with a grid size of 128^3.

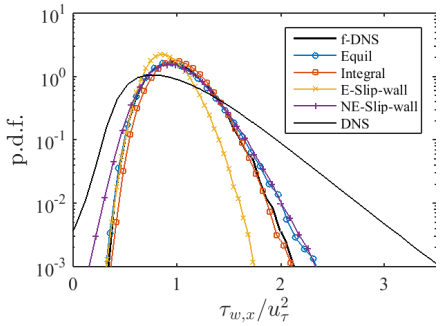

FIGURE 5. The streamwise wall stress PDF from WMLES, DNS and filtered DNS. f-DNS is filtered DNS. The other legends are the same as those in figure 2.

5. Log-layer mismatch

The log-layer mismatch refers to the mismatch between the stress from a WMLES calculation and that from a DNS calculation. Kawai & Larsson (2012) blamed LES errors at the first grid point from the wall for this mismatch and they proposed to use the second (or third, fourth) grid point away from the wall for the RANS-LES matching location. In an earlier investigation, Bou-Zeid *et al.* (2005) pointed out that even in the absence of LES errors, the equilibrium wall models would still lead to an over-predicted wall stress because $\langle \tau_{w,LES} \rangle \sim \langle u^2 \rangle > \langle u \rangle^2 \sim \langle \tau_w \rangle$, where u is the velocity at the first grid point and is assumed to be correctly modeled, τ_w is the real wall stress. To resolve this problem, Bou-Zeid *et al.* (2005) proposed to conduct a 2Δ filtering at the first grid

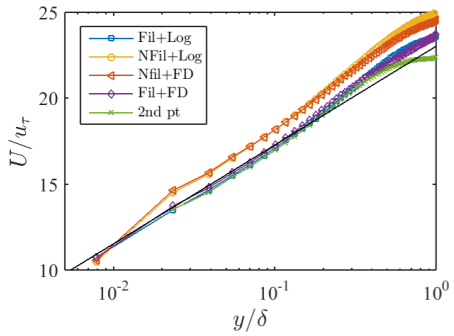

FIGURE 6. Mean velocity profile from various WMLES calculations. Fil is filtering at the first grid point, NFil is no filtering at the first grid point, Log is computing derivatives at the first grid point from the wall model, FD is computing derivatives at the first grid point using 2nd order finite difference (the same as in the bulk), 2nd pt is using the 2nd point for the wall model LES matching location.

point away from the wall. Both Kawai & Larsson (2012) and Bou-Zeid *et al.* (2005) were able to remove the log-layer mismatch.

In this section, the issue of log-layer mismatch is further investigated and both fixes from Kawai & Larsson (2012) and Bou-Zeid *et al.* (2005) are tested for channel flows using the code Lesgo. It worth note that, for all previous LES, the derivatives at the first grid point were computed from the wall model in Lesgo: $du_i/dy = u_\tau/(\kappa\Delta y_1) \times U_i/U$, where $i = 1, 3$, U_i is the LES velocity at the first grid point and $U = \sqrt{U_1^2 + U_2^2}$. The common practice is, however, to compute those derivatives in the same way they are computed in the bulk. To conform with the common practice, we have included results from LES that use regular finite difference for the derivatives at the frist grid point. The filtering used here is a 9-point top hat filtering.

In figure 6, the mean velocity profiles from various WMLES calculations are shown. All cases use a grid size of 64^3. We find first that a log-layer mismatch presents for regular implementation of equilibrium wall models and the stress is under-predicted (the flow rate is over predicted), second that computing the derivatives at the first grid point using the finite difference method or using the log law makes no difference, third that both filtering and using 2nd point for the wall model remove the mismatch. It is worth noting that the log-layer mismatch here is an under-prediction of the wall shear stress, instead of an over-prediction suggested by Bou-Zeid *et al.* (2005). In fact, $\left\langle {u_1'}^2 \right\rangle / \langle U_1 \rangle^2 = 4.3\%$ for Nfil+FD, where there is a mismatch, and $\left\langle {u_2'}^2 \right\rangle / \langle U_2 \rangle^2 = 4.1\%$ for 2nd pt, where there is no mismatch. The subscript 1, 2 denotes 1st or 2nd grid point from the wall. Those observations cannot be explained using the arguments presented in Bou-Zeid *et al.* (2005), calling for further investigation of the mechanism underlying the success of the filtering technique

6. Conclusions

In this work, a physics-based interpretation is provided for Robin-type LES wall closures. The slip-wall model, which is a direct consequence of using of the differetial filter in LES, is not entirely incompatible with other LES filters. For a WMLES of a canonical boundary layer, physically, the non-penetrating slip-wall closure is consistent with the algebraic equilibrium wall model. WMLES results suggest that the interpretation in

Section 2 is reasonable and the Robin-type wall closure, with a properly picked length scale l_p, can be used as an alternative to the conventional wall models that directly supply the wall shear stress. The performance of the algebraic equilibrium wall model, the algebraic integral wall model and the Robin-type wall model is compared in the context of turbulent channel flows. With sufficiently high resolution, the mean and the variance of the streamwise velocity fluctuations do not depend crucially on the choice of LES wall models, while for coarse-grid LES, the integral wall model and the slip-wall model have an advantage over the algebraic equilibrium wall model. Correct prediction of the PDF of the wall shear stress, on the other hand, depends very much on the choice of wall models. The study here indicates that for a channel flow at the particular Reynolds number studied ($\mathrm{Re}_\tau = 4200$), the integral wall model provides a nearly perfect prediction for the PDF of the filtered wall stress (filtered at the corresponding LES resolution). Whether this holds for a different flow configuration, at a different Reynolds number and at a different resolution is not entirely clear and further investigations are needed. As for the slip-wall models, explicitly accounting for the non-equilibrium effects helps predict the PDF of the wall shear stress.

To conclude the discussion, we briefly discuss how the effects of sub-grid roughness can be modeled in a Robin-type LES wall closure. In the pioneering work by Bose & Moin (2014), it is assumed that there is no roughness. Because the effects of roughness are commonly modeled with a $-C_d U^2$ term in the momentum equation, accounting for sub-grid roughness is non-trivial without referring to the NS equation. In this work, as we have connected the Robin-type wall condition to the NS equation, the effects of roughness can be accounted for by adding the drag term to Eq. (2.4) or simply by using an effective roughness length y_o in Eq. (2.5).

Acknowledgments

This investigation was funded by AFOSR and NASA.

REFERENCES

Anderson, W. & Meneveau, C. 2011 Dynamic roughness model for large-eddy simulation of turbulent flow over multiscale, fractal-like rough surfaces. *J. Fluid Mech.* **679**, 288–314.

Balaras, E. & Benocci, C. 1994 *Subgrid-scale models in finite-difference simulations of complex wall bounded flows.* AGARD CP 551.

Bazilevs, Y. & Hughes, T. J. 2007 Weak imposition of Dirichlet boundary conditions in fluid mechanics. *Comput. Fluids* **36**, 12–26.

Bose, S. & Moin, P. 2014 A dynamic slip boundary condition for wall-modeled large-eddy simulation. *Phys. Fluids* **26**, 015104.

Bou-Zeid, E., Meneveau, C. & Parlange, M. 2005 A scale-dependent Lagrangian dynamic model for large eddy simulation of complex turbulent flows. *Phys. Fluids* **17**, 025105.

Chapman, D. R. 1979 Computational aerodynamics development and outlook. *AIAA J.* **17**, 1293–1313.

Choi, H. & Moin, P. 2012 Grid-point requirements for large eddy simulation: Chapman's estimates revisited. *Phys. Fluids* **24**, 011702.

Chung, D. & Pullin, D. 2009 Large-eddy simulation and wall modelling of turbulent channel flow. *J. Fluid Mech.* **631**, 281–309.

Coles, D. 1956 The law of the wake in the turbulent boundary layer, *J. of Fluid Mech.*, **1**, 1956, 191–226.

Germano, M., Piomelli, U., Moin, P. & Cabot, W. H. 1991 A dynamic subgrid-scale eddy viscosity model. *Phys. Fluids* **3**, 1760–1765.

Graham, J., Kanov, K., Yang, X., Lee, M., Malaya, N., Lalescu, C., Burns, R., Eyink, G., Szalay, A., Moser, R. *et al.* 2016 A web services accessible database of turbulent channel flow and its use for testing a new integral wall model for LES. *J. Turbul.* **17**, 181–215.

Kawai, S. & Larsson, J. 2012 Wall-modeling in large eddy simulation: Length scales, grid resolution, and accuracy. *Phys. Fluids* **24**, 015105.

Lozano-Durán, A. & Jiménez, J. 2014 Effect of the computational domain on direct simulations of turbulent channels up to $\mathrm{Re}_\tau = 4200$. *Phys. Fluids* **26**, 011702.

Marusic, I., Monty, J. P., Hultmark, M., & Smits, A. J. 2013 On the logarithmic region in wall turbulence, *J. Fluid Mech.*, **716**, R3.

Meneveau, C., Lund, T. S. & Cabot, W. H. 1996 A Lagrangian dynamic subgrid-scale model of turbulence. *J. Fluid Mech.* **319**, 353–385.

Moeng, C.-H. 1984 A large-eddy-simulation model for the study of planetary boundary-layer turbulence. *J. Atmos. Sci.* **41**, 2052–2062.

Nicoud, F., Baggett, J., Moin, P. & Cabot, W. 2001 Large eddy simulation wall-modeling based on suboptimal control theory and linear stochastic estimation. *Phys. Fluids* **13**, 2968–2984.

Park, G. I. & Moin, P. 2014 An improved dynamic non-equilibrium wall-model for large eddy simulation. *Phys. Fluids* **26**, 015108.

Piomelli, U. & Balaras, E. 2002 Wall-layer models for large-eddy simulations. *Annu. Rev. Fluid Mech.* **34**, 349–374.

Porté-Agel, F., Meneveau, C. & Parlange, M. B. 2000 A scale-dependent dynamic model for large-eddy simulation: application to a neutral atmospheric boundary layer. *J. Fluid Mech.* **415**, 261–284.

Schumann, U. 1975 Subgrid scale model for finite difference simulations of turbulent flows in plane channels and annuli. *J. Comput. Phys.* **18**, 376–404.

Stevens, R., Wilczek, M. & Meneveau, C. 2014 Large-eddy simulation study of the logarithmic law for second- and higher-order moments in turbulent wall-bounded flow. *J. Fluid Mech.* **757**, 888–907.

Templeton, J. A., Wang, M. & Moin, P. 2006 An efficient wall model for large-eddy simulation based on optimal control theory. *Phys. Fluids* **18**, 025101.

Townsend, A. 1976 The structure of turbulent shear flow.Cambridge University Press.

Woodcock, J. & Marusic, I. 2015 The statistical behaviour of attached eddies. *Phys. Fluids* **27**, 015104.

Yang, X., Marusic, I. & Meneveau, C. 2016*a* Hierarchical random additive process and logarithmic scaling of generalized high order, two-point correlations in turbulent boundary layer flow. *Phys. Rev. Fluids* **1**, 024402.

Yang, X., Sadique, J., Mittal, R. & Meneveau, C. 2015 Integral wall model for large eddy simulations of wall-bounded turbulent flows. *Phys. Fluids* **27**, 025112.

Yang, X. I., Meneveau, C., Marusic, I. & Biferale, L. 2016*b* Extended self-similarity in moment-generating-functions in wall-bounded turbulence at high Reynolds number. *Phys. Rev. Fluids* **1**, 044405.